Journal of Turbulence
Vol. 00, No. 00, 200x, 1–14

RESEARCH ARTICLE

Core of the Magnetic Obstacle

E. V. Votyakov[a*] and S. C. Kassinos[a]

[a]Computational Science Laboratory UCY-CompSci
Department of Mechanical and Manufacturing Engineering,
University of Cyprus,
75 Kallipoleos, Nicosia 1678, Cyprus

(*Received 00 Month 200x; final version received 00 Month 200x*)

Rich recirculation patterns have been recently discovered in the electrically conducting flow subject to a local external magnetic termed "the magnetic obstacle" [Phys. Rev. Lett. 98 (2007), 144504]. This paper continues the study of magnetic obstacles and sheds new light on the core of the magnetic obstacle that develops between magnetic poles when the intensity of the external field is very large. A series of both 3D and 2D numerical simulations have been carried out, through which it is shown that the core of the magnetic obstacle is streamlined both by the upstream flow and by the induced cross stream electric currents, like a foreign insulated insertion placed inside the ordinary hydrodynamic flow. The closed streamlines of the mass flow resemble contour lines of electric potential, while closed streamlines of the electric current resemble contour lines of pressure. New recirculation patterns not reported before are found in the series of 2D simulations. These are composed of many (even number) vortices aligned along the spanwise line crossing the magnetic gap. The intensities of these vortices are shown to vanish toward to the center of the magnetic gap, confirming the general conclusion of 3D simulations that the core of the magnetic obstacle is frozen. The implications of these findings for the case of turbulent flow are discussed briefly.

Keywords: magnetohydrodynamics; low magnetic Reynolds number; magnetic obstacle; creeping flow; recirculation patterns

1. Introduction

A magnetic obstacle is a region in the flow of an electrically conducting fluid, e.g. liquid metal, where an external inhomogeneous magnetic field, $\mathbf{B}$, is applied as shown in Fig. 1*a*. The region of the magnetic obstacle manifests itself through the braking Lorentz force, $\mathbf{F_L} = \mathbf{j} \times \mathbf{B}$, originating from the interaction of $\mathbf{B}$ with electrical currents $\mathbf{j}$. The electrical currents are induced because of the electromotive force arising when the conducting liquid moves through the region of magnetic field. The net effect is that the core of the magnetic obstacle is impenetrable to the flow, much like a foreign solid insertion.

Characteristics of the flow influenced by a magnetic obstacle are of considerable fundamental and practical interest. On the fundamental side, such a system possesses a rich variety of dynamical states [1]. On the practical side, spatially localized magnetic fields enjoy a variety of industrial applications in metallurgy, e.g. [2], including stirring of melts by a moving magnetic obstacle (called electromagnetic stirring), removing undesired turbulent fluctuations during steel casting

*Corresponding author. Email: karaul@gmail.com

ISSN: 1468-5248 (online only)

DOI: 10.1080/14685240YYxxxxxxx
http://www.informaworld.com

using steady magnetic obstacles (called electromagnetic brake) and non-contact flow measurement using a magnetic obstacle (called Lorentz force velocimetry, e.g. [3]).

In this paper, the magnetic Reynolds number $R_m = \mu^* \sigma u_0 H$ is taken to be much less than one where μ^* is the magnetic permeability, σ is fluid electric conductivity, and u_0 and H are the characteristic scales for velocity and length. Therefore the induced magnetic field is expected to be much less that the imposed external magnetic field [4], [5], [6], [7]. Under this constraint, the external magnetic field has the following twofold effect on a turbulent magnetohydrodynamic (MHD) flow. Firstly, the turbulent velocity pulsations are suppressed in the direction parallel to the direction of the external field, that is the turbulence tends to be more and more two-dimensional when the external field becomes stronger and stronger [8], [9], [10]. This is true for the system subject to a homogeneous magnetic field where the mean velocity is constant over the flow except for boundary layers. Secondly, when the external field is local in space, as it must be in the case of the magnetic obstacle, then the decelerating Lorentz force is higher in the center of the obstacle compared to its periphery. This creates a shear gradient in the mean flow velocity which generates an additional vorticity which then diffuses downstream and contributes to the turbulence. Therefore it is important to understand for practical applications whether the useful turbulence-damping effect of a magnetic brake is not obliterated by excessive vorticity generation in the wake of the magnetic obstacle.

In order to deal with turbulent phenomena one needs to know the averaged parameters of the flow. However to properly define, for instance, the mean velocity is not a trivial task in the case of a local magnetic field because various recirculation patterns are possible both inside and in the vicinity of the magnetic obstacle as shown below. So the first obvious step is to study a laminar flow around the magnetic obstacle before attacking turbulence subject to the local external magnetic field. On the other hand, as shown in this paper and elsewhere [11], there is a similarity concept between a hydrodynamic flow around a solid cylinder and a MHD flow around a strong magnetic obstacle. This gives hope that numerous results for turbulent flows initiated by an obstacle can be projected onto turbulent MHD flows influenced by the local magnetic field. For instance, the vorticity generation by shear layer of a solid cylinder can be roughly perceived as similar to those in the shear layer alongside the magnetic obstacle. Thus, this paper is aimed to attract attention of researchers working on ordinary hydrodynamic turbulence to problems appearing in a MHD flow subject to a heterogeneous external magnetic field.

Studies of the effects of the magnetic obstacle on a liquid metal flow had been initiated in 1970s in the former Soviet Union by Gelfgat *et al.* [12], [13], and have been recently revived in the West by Cuevas *et al.* [14], [15], [16]. Among the above citations there were 2D numerical works related to creeping MHD flow, where a possible recirculation induced by the local magnetic was shown, see for example [12], [16], but where the physical explanation of the recirculation, as well as the generic scenario for the MHD flow around the magnetic obstacle, were obscured.

New results about the wake of a magnetic obstacle have been reported by [1], [17] and the generic scenario has been elaborated in [11]. It has been found that a liquid metal flow subject to a local magnetic field shows different recirculation patterns: (1) no vortices, when the viscous forces prevail at small Lorentz force, (2) one pair of *inner magnetic* vortices between the magnetic poles, when Lorentz force is high and inertia small, and (3) three pairs, namely, magnetic as above, *connecting* and *attached* vortices, when Lorentz and inertial forces are high. The latter six-vortex ensemble is shown in Fig. 1*b*.

The goal of the current paper is to highlight effects taking place in the laminar

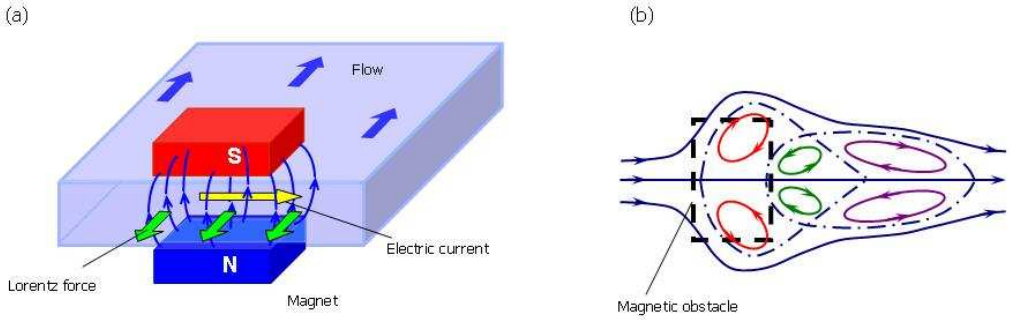

Figure 1. *a* - scheme of the magnetic obstacle created by two permanent magnets which are located on the top and bottom of the channel where an electrically conducting liquid flows. *b* - structure of the wake of the magnetic obstacle consisting of inner magnetic (first pair), connecting (second) and attached vortices (third pair). Dashed bold lines on *b* mark borders of the magnets.

flow around the magnetic obstacle when the interaction parameter N, which is a ratio of Lorentz force to the inertial force, increases. When N is very large, both mass transfer and electric field vanish in the region between magnetic poles. This region, hereinafter called the core of the magnetic obstacle, appears as if frozen by the external magnetic field, so that the upstream flow and crosswise electric currents can not penetrate inside it. Thus, the core of the magnetic obstacle is similar to a solid insulated obstacle inside an ordinary hydrodynamical flow with crosswise electric currents and *without* an external magnetic field. (This concerns hydrodynamics because there is no magnetic field, and the crosswise electric currents go around the insulated insertion without changing the mass flow.) Magnetic vortices are located aside the core and compensate shear stresses like a ball-bearing between the impenetrable region and upstream flow.

It is worthwhile to notice that the core of a magnetic obstacle is not similar to a stagnant region appearing in the MHD flow subject to a fringing transverse magnetic field. The fringing field is nonuniform in the streamwise direction and uniform in the spanwise direction, while in the case of the magnetic obstacle, the external local magnetic field is nonuniform in all the directions. Effects of the fringing field on a duct liquid metal flow have been intensively studied before, see for example [18], [19], [20], [21], [22], while those of the magnetic obstacle is a new research field [11]. It is trivial that in both cases the breaking Lorentz force is responsible for the phenomenon that the liquid metal flow vanishes in the space of the strong magnetic field. However, in the case of the fringing field the side flow jets are caused by a geometrical heterogeneity imposed by the sidewalls of the duct, and the stagnant region of vanishing flow tends to spread completely between the sidewalls. In the case of the magnetic obstacle, maxima of streamwise velocity appear in an originally free flow around the region where the magnetic field is of highest intensity, and the core roughly corresponds to the region where the magnetic field is imposed. The uniformity of the fringing field in the spanwise directions makes impossible recirculation in the M-shaped velocity profile, while magnetic vortices alongside a magnetic obstacle easily appear at moderate N [17].

The structure of the present paper is as follows. First, we present technical details of the simulations: model, equations and 3D numerical solver. Then, we report results for the core of the magnetic obstacle obtained in a series of 3D simulations. As an extension of the presentation given in TSFP-6 [23], we discuss also a 2D MHD flow and show the differences between 2D and 3D cases. A summary of the main conclusions ends the paper.

2. 3D Model: equations and numerical method

The equations governing the motion of an electrically conductive and incompressible fluid are derived from the Navier-Stokes equations coupled with the Maxwell equations for a moving medium and Ohm's law. By assuming that the induced magnetic field is infinitely small in comparison to the external magnetic field, the equations in dimensionless form are:

$$\frac{\partial \mathbf{u}}{\partial t} + (\mathbf{u}\cdot\nabla)\mathbf{u} = -\nabla p + \frac{1}{Re}\triangle\mathbf{u} + N(\mathbf{j}\times\mathbf{B}), \tag{1}$$

$$\mathbf{j} = -\nabla\phi + \mathbf{u}\times\mathbf{B}, \tag{2}$$

$$\nabla\cdot\mathbf{j} = 0, \tag{3}$$

$$\nabla\cdot\mathbf{u} = 0, \tag{4}$$

where $\mathbf{u}$ is velocity field, $\mathbf{B}$ is an external magnetic field, $\mathbf{j}$ is electric current density, p is pressure, ϕ is electric potential. The Reynolds number, $Re = u_0 H/\nu$, expresses a ratio between the inertia force and the viscous force and the interaction parameter, $N = B_0^2 H\sigma/(u_0\rho)$, expresses the ratio between the Lorentz force and the inertia force. Re and N are linked with each other by means of the Hartmann number, $Re\,N = Ha^2$, $Ha = HB_0(\sigma/\rho\nu)^{1/2}$, which determines the thickness δ of Hartmann boundary layers, $\delta/H \sim Ha^{-1}$, formed near the walls perpendicular to the direction of the magnetic field in the flow under constant magnetic field. Here, H is the characteristic length (size), u_0 is the characteristic flow velocity, B_0 the characteristic magnitude of the magnetic field intensity, ν is the kinematic viscosity of the fluid, σ is the electric conductivity of the fluid, and ρ is its density.

At given Re, N and $\mathbf{B}(x,y,z)$, the system of the partial differential equations shown above is solved in a 3D computational domain to obtain the unknown $\mathbf{u}(x,y,z)$, $p(x,y,z)$ and $\phi(x,y,z)$. The computational domain has periodical boundary conditions in the spanwise direction, and no-slip and insulating top and bottom walls (transverse direction). The electric potential at the inlet and outlet planes is taken equal to zero. For the velocity, the outlet boundary is force free, and a laminar parabolic velocity profile is imposed at the inlet boundary. We are interested in a stationary laminar solution, hence, the initial conditions play no role.

The origin of the right-handed coordinate system, $x = y = z = 0$, is taken in the center of the magnetic gap. The size of the computational domain is: $-L_x \le x \le L_x$, $-L_y \le y \le L_y$, $-H \le z \le H$, where $L_x = 25$, $L_y = 25$, $H = 1$ and x, y, z are respectively the streamwise, crosswise, and transverse directions.

The characteristic dimensions for the Reynolds number Re, and the interaction parameter N are the half-height of the duct H, the mean flow rate u_0, and the magnetic field intensity B_0 taken at the center of the magnetic gap, $x=y=z=0$. The range of the studied parameters is: $Re = 0.1, 1, 10, 100$ and $0 \le N \le 1000$.

The external magnetic field is modelled as a field from two permanent magnets occupying a space $\Omega = \{|x| \le M_x, |y| \le M_y, |z| \ge h\}$, where $M_x = 1.5$ ($M_y = 2$) is the streamwise (spanwise) width of the magnet, and $2 \times h$ is the distance between magnetic poles, $h = 1.5$. The magnets are supposed to be composed of magnetic dipoles oriented along the z-direction, therefore the total magnetic field $\mathbf{B}(x,y,z) = \int_\Omega \mathbf{B_d}(\mathbf{r},\mathbf{r}')d\mathbf{r}'$, where $\mathbf{B_d}(\mathbf{r},\mathbf{r}') = \nabla\left[\partial_z(1/|\mathbf{r}-\mathbf{r}'|)\right]$ is a field, at the point $\mathbf{r} = (x,y,z)$ created by the single magnetic dipole located in the point $\mathbf{r}' = (x',y',z')$. The integration can be performed analytically, see [17], and after

cumbersome algebraic calculations one obtains:

$$B_x(\mathbf{r}) = \frac{1}{B_0} \sum_{k=\pm1} \sum_{j=\pm1} \sum_{i=\pm1} (ijk) \operatorname{arctanh} \left[\frac{\delta_j}{\delta_{ijk}} \right],$$

$$B_y(\mathbf{r}) = \frac{1}{B_0} \sum_{k=\pm1} \sum_{j=\pm1} \sum_{i=\pm1} (ijk) \operatorname{arctanh} \left[\frac{\delta_i}{\delta_{ijk}} \right],$$

$$B_z(\mathbf{r}) = -\frac{1}{B_0} \sum_{k=\pm1} \sum_{j=\pm1} \sum_{i=\pm1} (ijk) \arctan \left[\frac{\delta_i \delta_j}{\delta_k \delta_{ijk}} \right],$$

where $\delta_i = (x - iM_x)$, $\delta_j = (y - jM_y)$, $\delta_k = (z - kh)$, and $\delta_{ijk} = [(x - iM_x)^2 + (y - jM_y)^2 + (z - kh)^2]^{1/2}$. The normalization factor B_0 is selected in such a way to have the intensity of the z-component equal one, $B_z(0, 0, 0) = 1$, in the center of the magnetic gap. Three-fold summation with the sign-alternating factor (ijk) reflects the fact that these equations are obtained by integrating over the 3D box Ω. Different cuts of the intensity $\mathbf{B}(\mathbf{r})$ are plotted in Fig. 3 and Fig. 4(b) in the paper of [17].

The 3D numerical solver has been explained in detail earlier, see [24]. It was developed from a free hydrodynamic solver originally created in the research group of Prof. M. Griebel ([25]). The solver employs the Chorin-type projection algorithm and finite differences on an inhomogeneous staggered regular grid. Time integration is done by the explicit Adams-Bashforth method that has second order accuracy. Convective and diffusive terms are implemented by means of the VONOS (variable-order non-oscillatory scheme) method. The 3D Poisson equations are solved for pressure and electric potential at each time step by using the bi-conjugate gradient stabilized method (BiCGStab).

The numerical grid was regular and inhomogeneous, $N_x \times N_y \times N_z = 64^3$. The minimal horizontal step size in the region of the magnetic gap was $\Delta x \simeq \Delta y \simeq 0.3$, which means that a few dozens points were used for resolving the inner vortices in the core of the magnetic obstacle. The minimal vertical step size near the top and bottom (Hartmann) walls was $\Delta z = 0.005$. This corresponds to using three to five $(= (1/Ha)/\Delta z)$ points to resolve Hartmann layer at $Ha = 40 - 70$. To ascertain that the numerical resolution was adequate, a few runs were performed with double the resolution and no differences have been found.

3. 3D results[11]

The goal of the simulations is to focus on the flow around a magnetic obstacle at large interaction parameter N. In order to achieve large $N = Ha^2/Re$, the simulations were started at a small interaction parameter and Ha was smoothly increased, while keeping Re constant. Several values of the Reynolds number were studied, $Re = 0.1, 1, 10, 100$, and no principal differences were found at the same N. These low values of Re imply low inertial forces, therefore, only two-vortex patterns were produced, without connecting and attached vortices.

In this Section, results are shown for the mid central plane, where all vortex peculiarities can be distinctively visualized. Nevertheless, it is necessary to note that the flow in the mid plane is not two-dimensional. There is a secondary flow from and into the mid plane towards and from the top and bottom walls. This secondary flow is caused by the process of creation and destruction of the Hartmann layers. 3D pictures of the vortices have been drawn before [17] and will not be

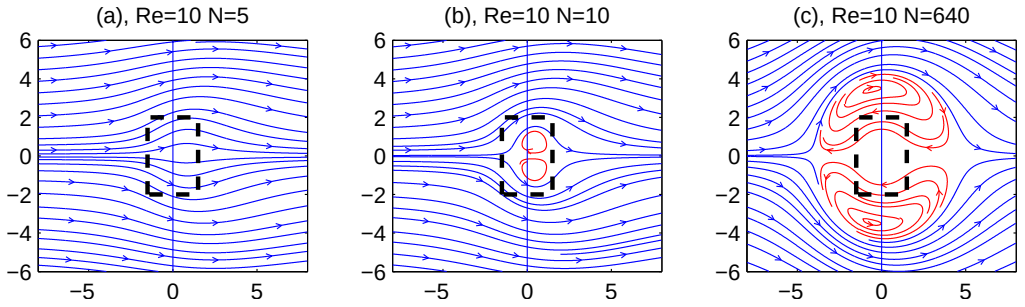

Figure 2. Streamlines in the central plane, $Re = 10$, N =5(a), 10(b), 640(c). Dashed bold lines mark borders of the magnets. As N gives rise, magnetic vortices move away each other by forming in between a core of the magnetic obstacle.

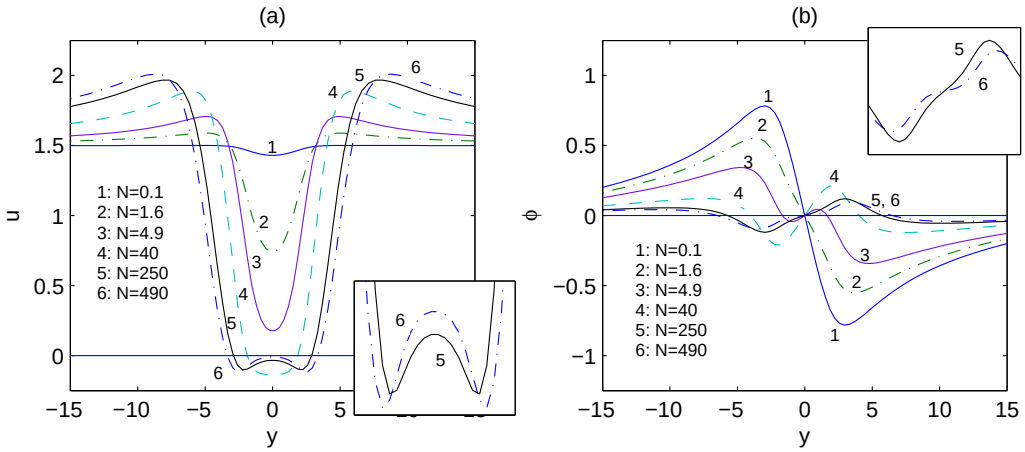

Figure 3. Streamwise velocity (a) and electric potential (b) along crosswise cuts of middle horizontal plane $x = z = 0$. $Re = 10$, N =0.1(solid 1), 1.6(dot-dashed 2), 4.9(solid 3), 40(dashed 4), 250(solid 5), and 490(dot-dashed 6). Insertion shows magnified plots for curves 5 and 6.

considered here.

The natural way to visualize the core of the magnetic obstacle is to plot streamlines of the flow in the central horizontal plane as shown in Fig. 2 at different interaction parameters N. Because N is the ratio of the Lorentz force to the inertial force, the larger N is, the stronger the retarding effect of the Lorenz force becomes. So, one observes no vortices at $N = 5$, Fig. 2a; weak circular magnetic vortices first appear at slightly below $N = 10$, as shown in Fig. 2b; and finally these vortices become well developed and strongly deformed at very large $N = 640$, Fig. 2c. In the latter case, the vortex streamlines envelop the bold dashed rectangle. This rectangle denotes the borders of the external magnet; inside the rectangle at large N one can see an island – the core of the magnetic obstacle. The observed deformation of the vortices and their drift from the center of the magnetic gap are due to the tendency of the flow to reduce the friction caused by retarding Lorentz force. The vortices are cambered and located in the shear layer alongside the magnetic gap in such a way that their rotation looks like the rotation of a ball-bearing inside the wheel.

The quantitative analysis of the core was performed by crosswise cuts through the center of the magnetic gap at different arising magnetic interaction parameters N. These cuts are shown in Fig. 3a for the streamwise velocity $u_x(y)$ and in Fig. 3b for the electric potential $\phi(y)$. First, we discuss how the streamwise velocity changes as N increases.

As shown in the Fig. 3a (curve 1), for small $N = 0.1$, the velocity profile is

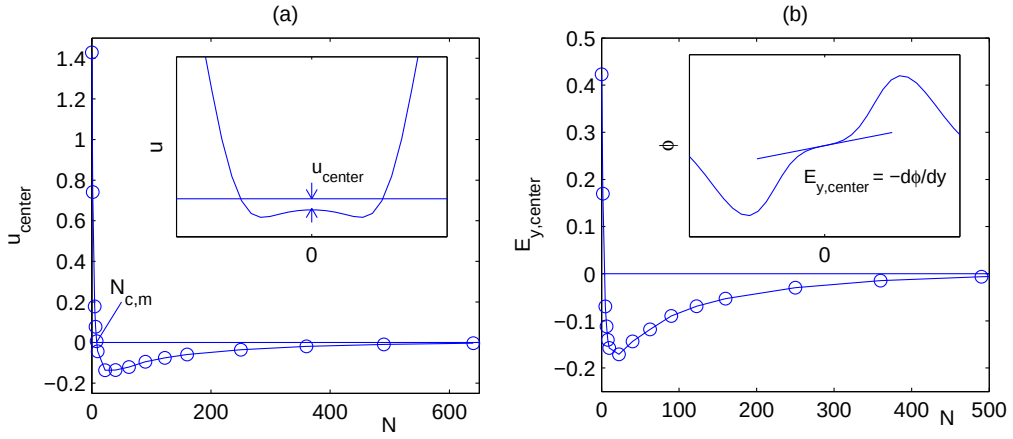

Figure 4. Central streamwise velocity u_{center} (a) and central spanwise electric field $E_{y,center}$ (b) as a function of the interaction parameter N. $N_{c,m}$ is a critical value where the streamwise velocity is equal to zero. Insertion shows the definition of u_{center} and $E_{y,center}$.

only slightly disturbed with respect to a uniform distribution. As N increases, the curves $u_x(y)$ pull further down in the central part $u_{center} \equiv u_x(0)$, see for example curves 2 and 3. At N higher than a critical value $N_{c,m}$, i.e. for curve 4, the central velocities u_{center} are negative. This means that there appears a reverse flow causing magnetic vortices in the magnetic gap. When N rises even more (see curves 5 and 6) the magnetic vortices become stronger and simultaneously shift away from the center to the side along the y direction, see insertion in Fig. 3a for curves 5 and 6.

Fig. 3(b) shows how the electric potential $\phi(y)$ varies along the central crosswise cut through the magnetic gap. The slope in the central point is the crosswise electric field, $E_{y,center} = -d\phi/dy|_{y=0}$. One can see that $E_{y,center}$ changes its sign: it is positive at small N and negative at high N. To explain why it is so, one can use the following way of thinking. Any free flow tends to pass over an obstacle in such a way so as to perform the lowest possible mechanical work, i.e. flow streamlines are the lines of least resistance to the transfer of mass. The resistance of the flow subject to an external magnetic field is caused by the retarding Lorentz force $F_x \approx j_y B_z$, so the flow tends to produce a crosswise electric current, j_y, as low as possible while preserving the divergence-free condition $\nabla \cdot \mathbf{j} = 0$. To satisfy the latter requirement, an electric field $\mathbf{E}$ must appear, which is directed in such a way, so as to compensate the currents produced by the electromotive force $\mathbf{u} \times \mathbf{B}$. Next, we analyze the crosswise electric current $j_y = E_y + (u_z B_x - u_x B_z)$. Due to symmetry in the center of the magnetic gap $B_y = B_x = u_y = u_z = j_y = j_z = 0$, so $j_y = E_y - u_x B_z$. This means that E_y tends to have the same sign as u_x in order to make j_y smaller. At small N, the streamwise velocity u_x is large and positive, so the electric field E_y is positive too. When the magnetic vortices appear, there is a reverse flow in the center. Therefore, the central velocity is negative now, and the central electric field $E_{y,center}$ is also negative.

The change of the electric field in the magnetic gap can be explained in terms of the Poisson equation and the concurrence between external and internal vorticity, see [17]. Those arguments are also valid here, however, in contrast to the previous study, we have no side walls now, so the external vorticity in the present case plays only a minor role. As a result, the reversal of the electric field appears at a small N (approximately equal to five), which is close to $\kappa = 0.4$ given in [17].

The overall data about u_{center} and $E_{y,center}$ in the whole range of N studied are shown in Fig. 4. One can see that both characteristics start from positive values, then, they cross the zeroth level, reach a minimum, go up again, and finally vanish

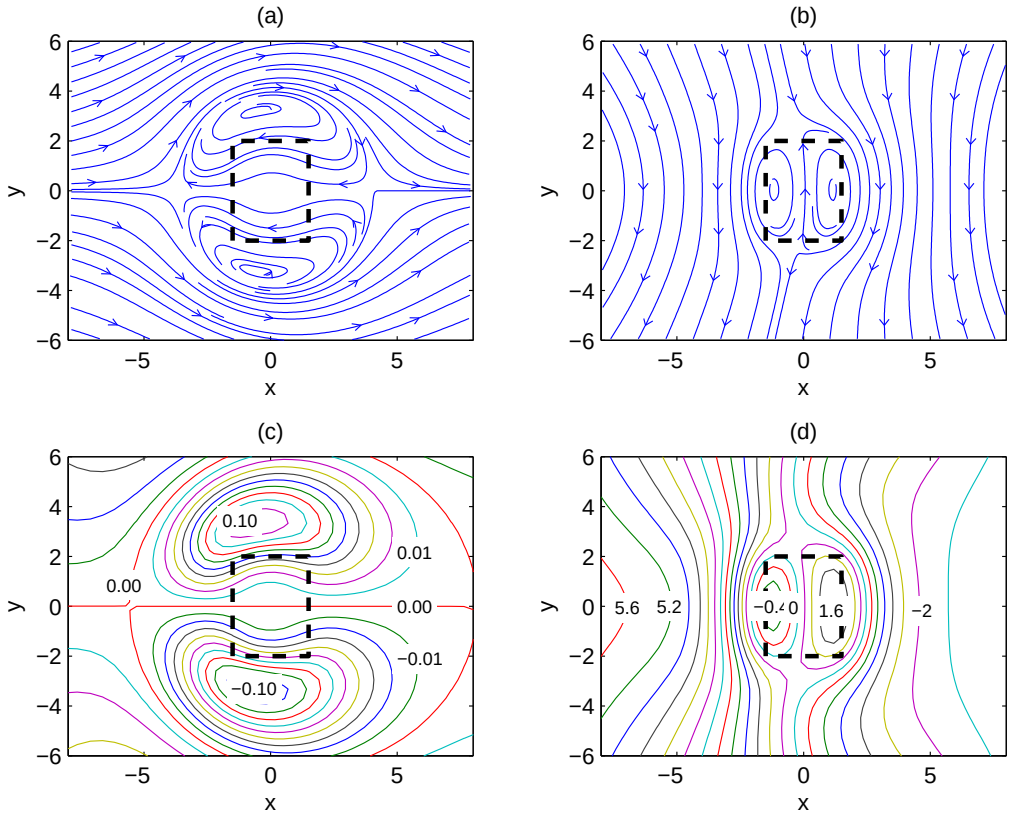

Figure 5. Middle horizontal plane, $z = 0$: streamlines of the mass (u_x, u_y) (a) and electric charge (j_x, y_y) (b) flow. Contour lines for the electric potential $\phi(x, y)$ (c) and pressure $p(x, y)$ (d) resemble the streamlines given above. $Re = 10$, $N = 490$. Contours of the electric potential are given with step 0.01, and contours of the pressure are given with the step 0.4. Dashed bold rectangle shows borders of the external magnet.

in the limit of high N. With respect to the streamwise velocity, this means that, at hight N, there is no mass flow in the center of the magnetic gap; the other velocity components are equal to zero due to symmetry. With respect to the crosswise electric field, this means that there are no electric currents. This occurs because there is no mass flow, therefore, the electromotive force vanishes, E_y goes to zero, and the other electric field components are equal to zero due to symmetry. Thus, one can say that the center of the magnetic gap is frozen by the strong external magnetic field, so that both mass flow and electric currents tend to bypass the center. In other words, this means that a strong magnetic obstacle has a core, and such a core is like a solid insulated body, being impenetrable for the external mass and electric charge flow.

When the inertia and viscous forces are negligible compared to the Lorentz force and pressure gradients, then mass flow streamlines must be governed by the electric potential distribution, while the trajectories of the induced electric current must be governed by pressure distribution. This is derived straightforwardly from equations (1 – 2). Because inertia and viscosity are vanishing, equations (1 – 2), in the core and nearest periphery of the magnetic obstacle, become:

$$\nabla p = \mathbf{j} \times \mathbf{B}, \quad \nabla \phi = -\mathbf{j} + \mathbf{u} \times \mathbf{B} \approx \mathbf{u} \times \mathbf{B}\,. \tag{5}$$

In the latter formula, $\mathbf{j} \ll \nabla\phi$ and $\mathbf{u} \times \mathbf{B}$ is the dominating term. In the core of the obstacle, $\mathbf{B} = (0, 0, B_z) \approx (0, 0, 1)$, hence, the pressure (electric potential) is a streamline function for the electric current (velocity), see Fig. 5. These relationships

for the flow under the strong external magnetic field had been discussed earlier by Kulikovskii in 1968 [26].

Kulikovskii's theory is linear, therefore, it must work well in the stagnant core of the magnetic obstacle. The traditional approach in the context of this theory is to introduce the so-called characteristic surfaces, and then, to impose Hartmann layers as boundary conditions for further integration along the characteristic surfaces. Such an approach has been used before for slowly varying fringing magnetic fields [19], where Hartmann layers and the inertialess assumption are reasonable. However, it is an open issue whether the concept of the characteristic surfaces is valid for the case of the magnetic obstacle. For perfectly electrically conductive liquids this concept forces mass and electric streamlines to flow along the surfaces of constant $\mathbf{B}$. The latter is the conjecture of (5) and is observed actually in Fig. $5a, b$ far from the core of the obstacle. Nevertheless, the concept of the characteristic surfaces does not allow for any recirculation in shear layers, what is the most remarkable effect here.

A magnetic field in a rotational flow requires more sophisticated boundary conditions than just the Hartmann layer. There is known a solution for the Ekman-Hartman layers [27], where both constant rotation and constant magnetic field are taken jointly into account. This probably does not fit the present case either, because the vorticity is not constant along the transverse direction, and the shape of vortices is not circular. Moreover, inclusion of the non constant vorticity destroys the linearity of Kulikovskii's theory. Therefore, Kulikovskii's theory could not be used as it stands to predict recirculation a priori. Indeed, this explains why the theory has not been applied to magnetic vortices, even though it has been known for a while. Nevertheless, Kulikovskii's theory is useful and must be mentioned because it explains a posteriori the shape of vortices and their matching to electric potential lines.

4. 2D creeping flow around magnetic obstacle

It is interesting to compare our results with those reported earlier by Cuevas *et.al* [16] for a creeping 2D MHD flow. In particular, these authors observed not only two magnetic vortices, but four vortices as well as, aligned in the spanwise direction at high Hartmann numbers, see Fig. 9 of [16]. The four-vortex aligned structure has been missed in our 3D simulations, therefore to get insight about it, we have performed our own 2D simulations with the same parameters for the magnetic field $M_x = 0.5$, $M_y = 0.5$, $h = 1$ (our formula for the field (5) coincides with Eq. (31) of [16]) and $Re = 0.05$. To gather more information, we explored the larger Ha range, $0 \leq Ha \leq 150$. A 2D finite element method[1] was numerically employed to solve the vorticity-stream function formulation of steady-state Navier-Stokes equation with the Lorentz force. Electric currents were calculated from the magnetic induction equation. Generally, the obtained 2D results coincided with those from [16] and also extended them as reported below.

The main curve of our 2D results is presented in Fig. 6. It shows the dependence of the velocity in the center of the magnetic obstacle as a function of Ha number. (This is similar to Fig. $4(a)$ with the difference that the x-axis corresponds to Ha instead of N.) One can see that u_{center} vanishes as Ha increases, i.e. mass flow disappears in the core of the obstacle as the intensity of the magnetic field gives rise. Therefore, the principal conclusion derived from 3D results remains valid:

[1] In the 2D simulations, the numerical mesh varied from 64^2 to 256^2. The quality of the mesh was checked by repeating the runs with doubled resolution.

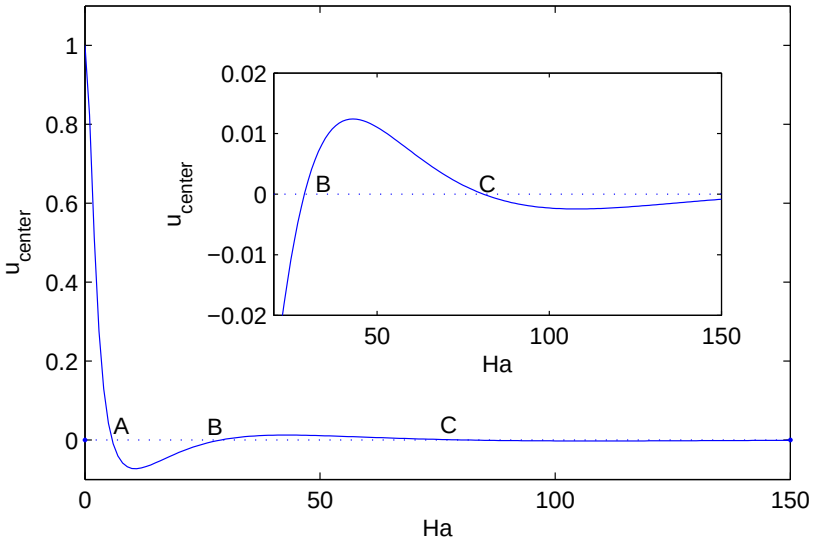

Figure 6. Central streamwise velocity u_{center} as a function of Ha for 2D MHD flow, $Re = 0.05$, $M_x = 0.5$, $M_y = 0.5$, $h = 1$. Insertion is the zoom for $20 \leq Ha \leq 150$.

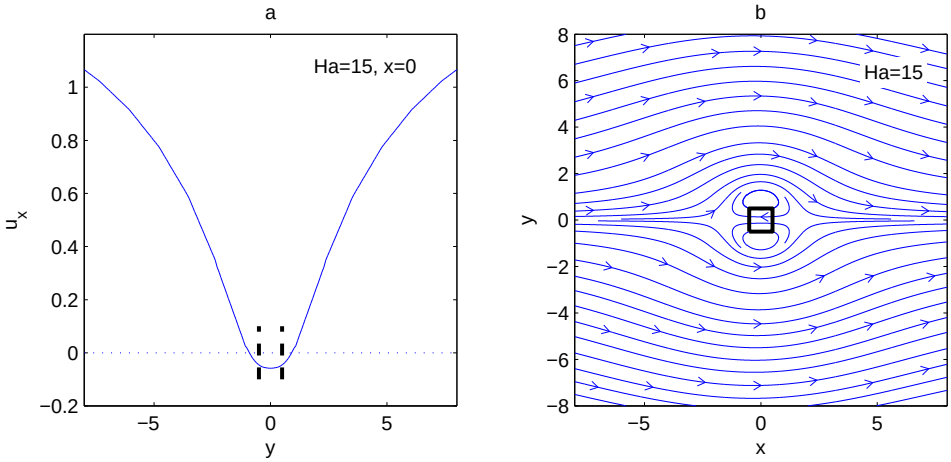

Figure 7. Streamwise velocity u_x along spanwise direction at $x = 0$ (a) and flow streamlines (b) at $H = 15$ for 2D MHD flow. On (b) one distinguishes two magnetic vortices. Bold lines denote borders of the magnet.

there develops a frozen core of the magnetic obstacle when Ha is large. However, the details of the to approach zero-level values for u_{center} are different in 2D case relative to the 3D case. To stress this fact, we zoomed the curve in Fig. 6 and put it as an insertion. One can see that in the 2D case u_{center} vanishes with oscillations, while in the 3D case, see Fig. 4(a), it was always negative as it approaching the zero level.

To consider in detail the different flow regimes shown cumulatively in Fig. 6, we have labelled the turning points, where u_{center} changes its sign, with the letters A,B,C. Figures 7-9 illustrate below three nontrivial flow regimes through two plots: the streamwise velocity profile along the central spanwise line, $x = 0$, and flow streamlines.

The first regime, corresponding to the Ha range from zero up to the first turning point, A, is characterized by a weak breaking Lorentz force. There is no recirculation, so we have considered this regime as trivial, and did not illustrate it further by any figure. It is marked as regime I and represented by Fig. 7 in the paper by

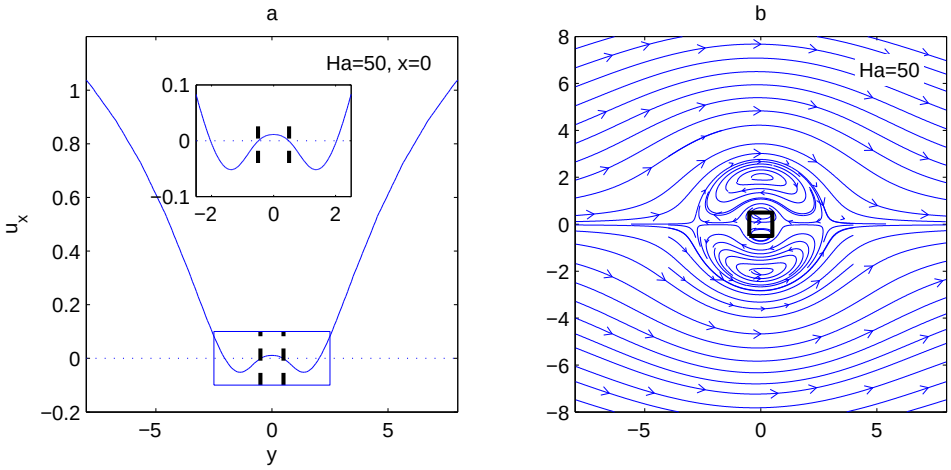

Figure 8. Streamwise velocity u_x along spanwise direction at $x = 0$ (a) and flow streamlines (b) at $H = 50$ for 2D MHD flow. Insertion on (a) is the zoom for $-1.5 \leq y \leq 1.5$. On (b) one distinguishes four vortices aligned along the y direction at $x = 0$. Bold lines denote borders of the magnet.

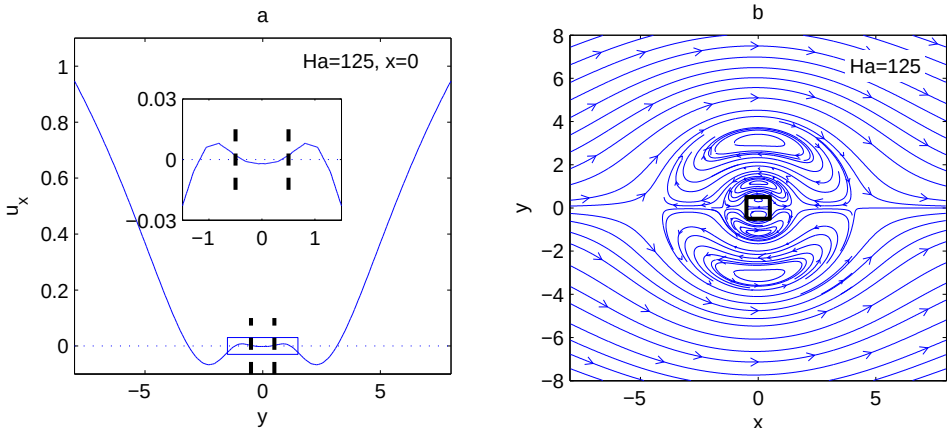

Figure 9. Streamwise velocity u_x along spanwise direction at $x = 0$ (a) and flow streamlines (b) at $H = 125$ for 2D MHD flow. Insertion on (a) is the zoom for $-1.5 \leq y \leq 1.5$. On (b) one distinguishes six vortices aligned along the y direction at $x = 0$. Bold lines denote borders of the magnet.

Cuevas *et al.* [16].

The second regime is for the Ha interval between the first turning point, A, and the second, B. It is characterized by a Lorentz force that is already strong enough, to reverse the flow between the magnetic poles. This results in two magnetic vortices as illustrated by Fig. 7 of the current paper and Fig. 8 of [16]. These vortices are analogous to those in 3D results, with the difference that in the 3D simulation the flow particles captured by the magnetic vortices move helically towards the top and bottom walls to dissipate upstream kinetic energy [17], while in the 2D system they always follow rotation along closed contour lines of the stream function.

In the third regime, for the Ha range between turning points B and C, the reversal of the upstream flow occurs in the shear layer rather than in the center of the magnetic obstacle. This can be explained by the fact that, at these Ha, the flow in the core is hindered, and the shear layer between the core and the bypassing flows is large to accommodate magnetic vortices. When this happens, the requirement of flow continuity, $\nabla \mathbf{u}_\perp = 0$, turns the velocity in the center of the obstacle to positive values. As a result, the four vortex, aligned along the central spanwise line, appear as shown in Fig. 8 (see also Fig. 9 of [16]).

When Ha increases further, after the turning point C, the shear layer is extended

further as well. So the whole elongated vortex structure increases in length, and two vortices, that were closest to the center of the stagnant core, are pushed out from the core. Again, to satisfy flow continuity this initiates the weaker counter-rotating vortices in the core. In this regime, there are altogether six aligned vortices shown in Fig. 9. This recirculation pattern is new and has not been reported earlier.

Now, we can offer the following qualitative description of the creeping 2D MHD flow around a magnetic obstacle. As Ha increases more and more, additional vortices appear in the expanded shear layer. These vortices have decaying intensity towards to the magnetic gap and are alternating-signed, starting from the very first vortex, counted from the bypassing flow, where the flow is reversed. This results in vanishing velocity oscillations in the center of the magnetic gap, Fig. 6.

The question arises whether the aligned multi-vortices appear in a creeping 3D MHD flow. In the latter case, the largest N under consideration was 1000 and two magnetic vortices were observed only. The four-vortex aligned structure that was clearly presented in our 2D results, occurred at $Ha \approx 50$, which corresponds to ($Re = 0.05$) $N = Ha^2/Re = 50000$, much larger than the maximum $N = 1000$ used in the 3D simulations. On the other hand, the velocities are of magnitude $10^{-3} - 10^{-2}$ at the center of the magnetic gap, so one would have to employ a very accurate 3D numerical code to verify the effect discussed.

Physically, the crucial difference between 2D and 3D vortices is the secondary flow in the transverse direction. This dissipates kinetic energy of the upstream flow inside viscous boundary layers located on no-slip top/bottom walls of the duct. On the other hand, the secondary flow variation, $\partial_z u_z$, is a mass source/sink adjusted to keep flow continuity, $\nabla_\perp \mathbf{u}_\perp = -\partial_z u_z$. Obviously in 2D cases, the dissipation by the secondary flow is absent and the flow is obliged to satisfy 2D continuity, $\nabla_\perp \mathbf{u}_\perp = 0$. Then, the possible way to dissipate energy and the flow be continuous in 2D is to create a weaker counter-rotating vortex nearby a strong vortex, the phenomena observed in Fig. 8 and 9.

5. Core of the magnetic obstacle and controlled production of vorticity.

It is worth to discuss how a magnetic obstacle can be used to control vorticity and turbulence. On the one hand, the magnetic field damps turbulent pulsations in the core of the obstacle by freezing any kind of mass and electric transfer. On the other hand, the shear layer between the core of the obstacle and the rest of the flow generates a transverse vorticity. The results presented herein were obtained at low Re numbers, and all the vortices were confined in the shear layer. However, it is possible to imagine the following two scenarios. The first situation is to destroy the initial core by increasing the Re number, that is by turbulating the flow, at fixed magnetic field parameters; and the second situation is to increase the magnetic field strength so as to manifest the core, that is to laminarize the core, while the Re number remans high and the rest of the flow is turbulent.

In the trivial turbulating scenario, the interaction parameter $N = Ha^2/Re$ is initially high because of the Re number being low while the Ha number is moderate[1] Then, one increases the Re, which could be equivalent to increasing the inlet flow rate. Obviously, since Ha is fixed, a higher Re implies a lower N, hence, the core of the magnetic obstacle becomes more penetrable, so the lateral magnetic vortices will shift toward each other due to the unfreezing of the core. At some threshold Re number, when the inertia of the flow becomes sufficiently high to

[1] A moderate Ha number range was also used in this paper in order to avoid numerical difficulties related to the resolution of Hartmann layers.

produce a stagnant region behind the core of the obstacle, one will have to observe the six-vortex pattern shown schematically in Fig. 1. Then, an even higher Re number will result in the detachment of the attached vortices (the third pair of vortices in Fig. 1) which is analogous to the classical process of the detachment of the attached vortices past solid cylinder [11]. Finally, at the highest Re, the interaction parameter N will become so small that the internal recirculation structure of the magnetic obstacle will disappear, and the flow will become turbulent as in the ordinary hydrodynamics.

In the laminarizing scenario, by taking initially a high Re number and keeping it fixed, one increases the Ha number by imposing, for instance, an external local magnetic field with higher and higher intensity. This increases the interaction parameter N, so the core of the obstacle must manifest itself by first showing the same six-vortex recirculation as aforementioned. In practice however, it might be difficult for all six vortices to be stable at very high Re, because in this case the rest of the flow is turbulent, so the wake of the obstacle oscillates and can potentially destroy the stability of the connecting and attached vortices (the second and the third pair of the vortices in Fig. 1). Nevertheless, the lateral magnetic vortices (the first pair of the vortices in Fig. 1) must manifest themselves clearly at any Re provided that N is large. These vortices will be distinctly seen at the beginning of the turbulent wake. A further increase of the Ha does laminarize and freeze the core of the obstacle. The magnetic vortices move away from each other and adjust their position in the lateral shear layers. Owing to the high Re number, the recirculation confined in the shear layer possesses an excess amount of kinetic energy that is dissipated downstream in the wake of the obstacle.

In the case of a solid obstacle one has little control over the shear layer at high Re because there is one parameter only, i.e. Re. Also, the solid obstacle is impenetrable and could not fit itself to the flow. In the case of the magnetic obstacle one has an opportunity to govern the detachment process because there are two additional parameters at a given Re: the Ha number, for instance, the magnetic field intensity controlling the degree of permeability of the magnetic obstacle; and the degree of lateral heterogeneity of the external magnetic field controlling the width of the lateral shear layer. Thus, a controlled intensity and shape of a magnetic obstacle is a model lab to produce and study vorticity generation and turbulent phenomena.

6. Conclusions.

3D numerical simulations are reported for a liquid metal flow subject to a strong external heterogenous magnetic field. The simulations shed light on the process of formation of the core of the magnetic obstacle when the interaction parameter N is large. The core is surrounded by deformed magnetic vortices located in the shear layer. Inside the core, there is no mass and electric transfer, i.e. at high N, the magnetic obstacle is analogous to a solid hydrodynamical obstacle.

The series of 2D simulations for a creeping MHD flow demonstrated that there still exists a weak recirculation in the stagnant core in 2D cases even at very high Ha. The flow regime can be represented as an elongated recirculation composed of many (even number) sign-alternating vortices aligned along the line crossing the center of the magnetic gap in the spanwise direction. The intensity of vortices vanishes by approaching the core of the magnetic obstacle, therefore, the principal conclusion derived from 3D results remains valid: there develops a frozen core of the magnetic obstacle when Ha grows toward infinity. By studying the characteristics of magnetic obstacles in laminar flow, we have been able to provide conjectures on the formation and destruction of magnetic obstacle in turbulent flow.

7. ACKNOWLEDGEMENTS

This work has been performed under the UCY-CompSci project, a Marie Curie Transfer of Knowledge (TOK-DEV) grant (Contract No. MTKD-CT-2004-014199). This work was also partially funded under a Center of Excellence grant from the Norwegian Research Council to the Center of Biomedical Computing.

References

[1] E.V. Votyakov, Y. Kolesnikov, O. Andreev, E. Zienicke, and A. Thess, *Structure of the wake of a magnetic obstacle*, Phys. Rev. Lett. 98 (2007), p. 144504.
[2] P. Davidson, *Magnetohydrodynamics in Materials Processing*, Annual Review of Fluid Mechanics 31 (1999), pp. 273–300.
[3] A. Thess, E.V. Votyakov, and Y. Kolesnikov, *Lorentz Force Velocimetry*, Phys. Rev. Lett. 96 (2006), p. 164501.
[4] J.A. Shercliff *The theory of electromagnetic flow-measurement*, Cambridge University Press, 1962.
[5] P.H. Roberts *An introduction to Magnetohydrodynamics*, Longmans, Green, New York, 1967.
[6] R. Moreau *Magnetohydrodynamics*, Kluwer Academic Publishers, Dordrecht, 1990.
[7] P.A. Davidson *An introduction to Magnetohydrodynamics*, Cambridge University Press, 2001.
[8] H.K. Moffatt, *On the suppression of turbulence by a uniform magnetic field*, J. Fluid. Mech. 28 (1967), pp. 571–592.
[9] J. Sommeria, and R. Moreau, *Why, how, and when, MHD turbulence becomes two-dimensional*, J. Fluid. Mech. 118 (1982), pp. 507–518.
[10] P.A. Davidson, *The role of angular momentum in the magnetic damping of turbulence*, J. Fluid. Mech. 336 (1997), pp. 123–150.
[11] E.V. Votyakov, and S.C. Kassinos, *On the analogy between streamlined magnetic and solid obstacles*, Phys. Fluids 21 (2009), pp. 097102–11.
[12] Y.M. Gelfgat, D.E. Peterson, and E.V. Shcherbinin, *Velocity structure of flows in nonuniform constant magnetic fields 1. Numerical calculations.*, Magnetohydrodynamics 14 (1978), pp. 55–61.
[13] Y.M. Gelfgat, and S.V. Olshanskii, *Velocity structure of flows in non-uniform constant magnetic fields. II. Experimental results.*, Magnetohydrodynamics 14 (1978), pp. 151–154.
[14] S. Cuevas, S. Smolentsev, and M. Abdou, *Vorticity generation in non-uniform mhd flows*, in *Proceedings of the Joint 15th Riga and 6th PAMIR International Conference. Fundamental and Applied MHD*, Vol. 1, Riga, Jurmala, Latvia, June 27-July 1, 2005, pp. 25–32.
[15] S. Cuevas, S. Smolentsev, and M. Abdou, *On the flow past a magnetic obstacle*, J. Fluid. Mech. 553 (2006), pp. 227 – 252.
[16] S. Cuevas, S. Smolentsev, and M. Abdou, *Vorticity generation in creeping flow past a magnetic obstacle*, Phys. Rev. E 74 (2006), p. 056301.
[17] E.V. Votyakov, E. Zienicke, and Y. Kolesnikov, *Constrained flow around a magnetic obstacle*, J. Fluid. Mech. 610 (2008), pp. 131–156.
[18] S. Molokov, and C.B. Reed, *Parametric Study of the Liquid Metal Flow in a Straight Insulated Circular Duct in a Strong Nonuniform Magnetic Field*, Fusion Science And Technology 43 (2003), pp. 200–216.
[19] T. Alboussiere, *A geostrophic-like model for large Hartmann number flows*, J. Fluid. Mech. 521 (2004), pp. 125–154.
[20] H. Kumamaru, S. Kodama, H. Hirano, and K. Itoh, *Three-Dimensional Numerical Calculations on Liquid-Metal Magnetohydrodynamic Flow in Magnetic-Field Inlet-Region*, Journal of Nuclear Science and Technology 41 (2004), pp. 624–631.
[21] H. Kumamaru, K. Shimoda, and K. Itoh, *Three-Dimensional Numerical Calculations on Liquid-Metal Magneto-hydrodynamic Flow through Circular Pipe in Magnetic-Field Inlet-Region*, Journal of Nuclear Science and Technology 44 (2007), pp. 714–722.
[22] M. Ni, R. Munipalli, P. Huang, N.B. Morley, and M.A. Abdou, *A current density conservative scheme for incompressible MHD flows at a low magnetic Reynolds number. Part II: On an arbitrary collocated mesh*, Journal of Computational Physics 227 (2007), pp. 205–228.
[23] E.V. Votyakov, and S.C. Kassinos, *Core of the magnetic obstacle*, in *The sixth International Symposium on Turbulence and Shear Flow Phenomena, Vol.II*, Seoul, Repeublic of Korea, 2009, pp. 703–707.
[24] E.V. Votyakov, and E. Zienicke, *Numerical study of liquid metal flow in a rectangular duct under the influence of a heterogenous magnetic field*, Fluid Dynamics & Materials Processing 3 (2007), pp. 97–113.
[25] M. Griebel, T. Dornseifer, and T. Neunhoeffer *Numerische Strömungssimulation in der Strömungsmechanik*, Vieweg Verlag, Braunschweig, 1995.
[26] A. Kulikovskii, *Slow steady flows of a conducting fluid at high Hartmann numbers*, Izv. Akad. Nauk. SSSR Mekh. Zhidk. i Gaza (1968), pp. 3–10.
[27] L. Debnath, *On Ekman and Hartmann Boundary Layers in a Rotating Fluid*, Acta Mechanica 18 (1973), pp. 333–341.